Chapter 1

Introduction

Part of this chapter is published as 'Gurudeo Nirala, Dharmendra Yadav & Shail Upadhyay; Ruddlesden-Popper phase A_2BO_4 oxides: Recent studies on structure, electrical, dielectric, and optical properties; *J. Adv. Ceram.* **9**, 129–148 (2020).'

1.1 Perovskites: Structural Diversity

The first natural perovskite, CaTiO3, was discovered in 1839 by German scientist and mineralogist Gaustav Rose, and is now known as perovskite after Lev Alexeievitch Perovsky [1]. The usual chemical formula for this family is ABX_3, with A and B being cations and X being an anion, which can be oxygen or halide group elements. It is assumed that the valence of A and B is such that the charge of anions can compensate for it. The majority of elements connected in the form of (A^{3+} - B^{3+}), (A^{2+} - B^{4+}), (A^{+} - B^{5+}), from the periodic table, for example: $LaAlO_3$, $BaSnO_3$, $KNbO_3$, etc., have perovskite structures. The BO_6 octahedra framework, which is created by the sharing of oxygen at the corner, can be used to characterise the perovskites' structure. The A atom is positioned at the cube's corner and shared by eight octahedra, but B is located at the cube's body centred position and oxygen is present at the face of each cubic face, generating an octahedra by B-cation, as shown in Fig. 1.1. The perovskite structure can also be defined as an AO rock salt layer interconnected by two layers of BO_2 from above and below to characterise the layer structure. The perovskite structure is one of the most adaptable structures, allowing for the development of a huge variety of phases with completely different capabilities by modifying the structure [2].

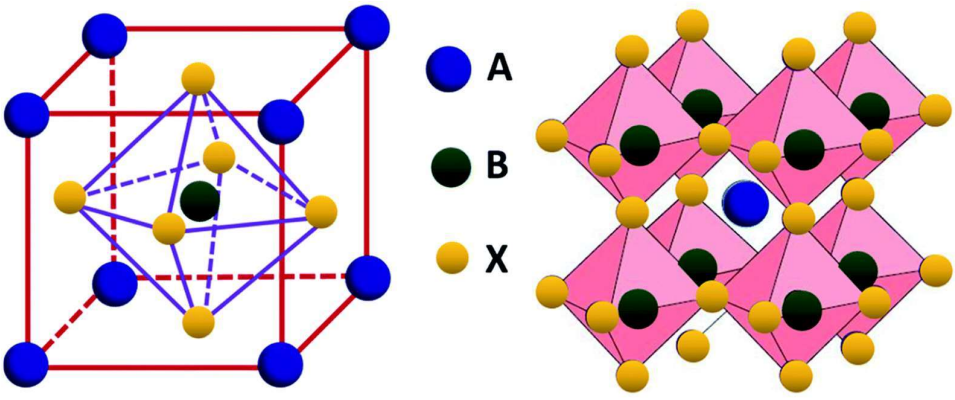

Figure 1.1. A unit cell of ABO_3 type cubic perovskite oxide structure.

Due to enormous flexibilities in Perovskites structure and its compositions, the distortion produced due to cationic substitution is tolerable in the structure. The degree of

mismatch between the AO and BO_2 layers (measured by ionic radii mismatch) determine perovskite structural tolerance [3]. The precise geometrical match between the AO and BO_2 layers produces an excellent perovskite structure. The following is the equation that determines geometric consistency:

$$r(A-O) = \sqrt{2}\, r(B-O) \qquad (1.1)$$

The distances $r(A-O)$ and $r(B-O)$ are computed from the ionic radii of the corresponding atoms. The "Tolerance Factor (t)" is a term used to describe structure persistence. It was first introduced by Goldschmidt, and it may be expressed mathematically as [3];

$$t = \frac{r_A + r_O}{\sqrt{2}\,(r_B + r_O)} \qquad (1.2)$$

where, r_A, r_B, and r_O are the ionic radii of cation A, B, and anion O, respectively. Depending on the tolerance factor, several crystal shapes are possible; for example, $t = 1$ produces a perfect cubic structure. The different crystal structures and associated tolerance factors are listed in Table 1.1.

Table 1.1. Tolerance factor of different crystal structure.

Goldschmidt tolerance factor (t)	**Structure**	**Explanation**	**Example**
>1.0	Hexagonal or Tetragonal	A ion is too big or B ion is too small.	$BaTiO_3$ [4]
0.90-1.00	Cubic	A and B ions have ideal size.	$BaSnO_3$ [4] $BaTiO_3$ [5]
0.71 - 0.90	Orthorhombic/Rhombohedral	A ion is too small to fit into B ion interstices.	$GdFeO_3$ [4] $CaTiO_3$ [4,6]
<0.71	Triclinic/Monoclinic	A ions and B have similar ionic radii.	Ilmenite, $FeTiO_3$ [7]

1.2 Ruddlesden D Popper (RP) Oxide Phase

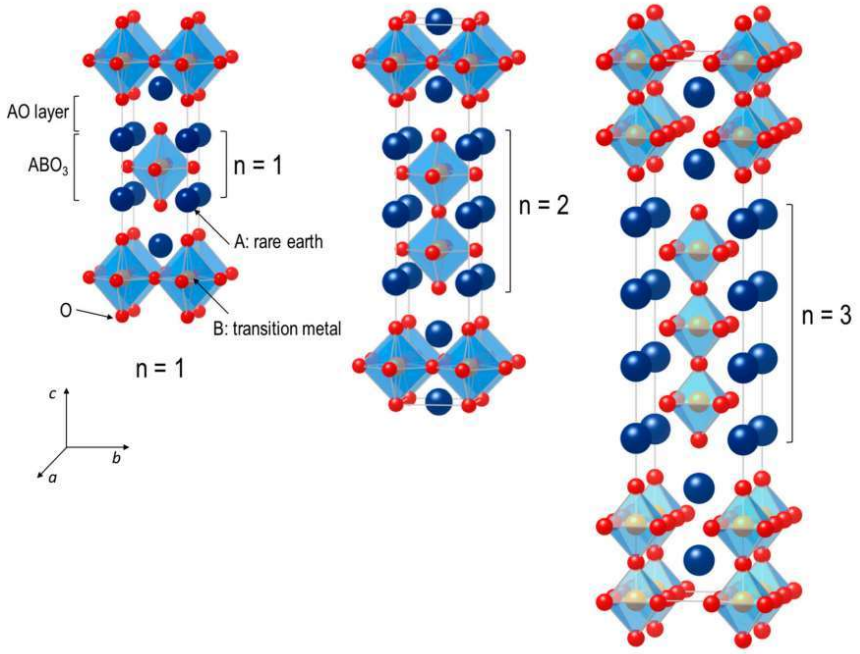

Figure 1.2. Schematic crystal structures of n = 1, 2 and 3 members of Ruddlesden–Popper type $A_{n+1}B_nO_{3n+1}$ [8].

Perovskite structural variety is enhanced due to high tolerance in the perovskite structure at low dimensionality. As seen in the layered representation of perovskite structure, the parent structure of the perovskite phase is made up of alternate stacking of AO and BO_2 layers (Fig. 1.1). This stack can be disrupted by intergrowth entities due to flexibilities of these structures, and it can sustain a wide range of dopant intergrowth (in terms of being off set in position and sequence). These findings, which were seen in a variety of homologous series and structural families, are fascinating. All of these formations are referred to as layered perovskite. Ruddlesden Popper, Dion–Jacobson, Aurivillius phases, and a broad family of high-temperature superconducting cuperates are examples of layered perovskites [9]. The Ruddlesden Popper (RP) series is a well-known and fundamental layered perovskite in which an extra layer of AO breaks the alternating $AO - BO_2$ stacking. As a result, the Ruddlesden

Popper oxide can be written as $AO(AO-BO_2)_n$ or $A_{n+1}B_nO_{3n+1}$, where $n = 1$ in A_2BO_4, and $n = 2$ in $A_3B_2O_7$, and so on (see Fig. 1.2).

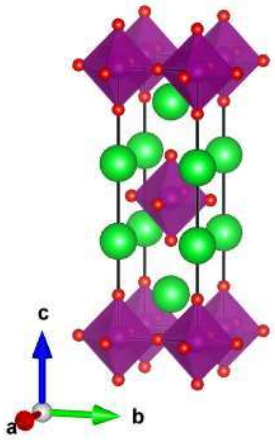

Figure 1.3. Ideal tetragonal unit cell of stoichiometric A_2BO_4 layered perovskite crystalized in I4/mmm space group.

The above formula $A_{n+1}B_nO_{3n+1}$ can also be written as $AO(ABO_3)_n$, where n perovskite layers are stacked between AO rock-salt layers along the crystallographic c-axis [10]. The first member of the series, A_2BO_4 ($n = 1$), adopts the K_2NiF_4 structure. Fig. 1.3 represents the ideal tetragonal unit-cell of a RP-phase A_2BO_4 oxide, which corresponds to the stoichiometric compound crystalized in $I4/mmm$ space group. This is also a two-dimensional (2D) layered perovskite structure. Commonly, A_2BO_4 oxides consist of rare or alkaline earth element as A-site cations with transition or post-transition metals on the B-site, forming an extensive series of compositions. The A-site cations have a coordination number of '9', locating at the boundary between the two types of layers, while the B-site cations are positioned at the center of an octahedron formed by six oxygen anions. RP oxides have shown very attractive and versatile physical properties such as superconductivity [11–15], magnetoresistance [16–20], mixed ionic and electronic conductivity [21–24], giant and colossal dielectric [25–28], low loss microwave dielectric [29–33], photoluminescence [34–38], catalytic activity [39–41], thermoelectric [42–44], etc., which are useful for many energy and electronic devices. The

A_2BO_4 layered perovskites have recently attracted attention owing to their great environmental stability and versatile applications. The alkaline earth element (AE) doped and undoped RE_2MO_4 layered perovskites (where RE is rare earth element and M is transition metal) and alkaline earth elements (AE) doped oxides have been considered as alternatives for cathode application in Solid Oxide Fell Cells (SOFC)/Solid Oxide Electrolysis Cells (SOEC), due to their superior mixed ionic and electronic conductivities in comparison to traditionally used perovskite oxides [45–48]. Sr_2CeO_4, AE_2SnO_4 ($AE = Ca, Sr, Ba$) is found to be a suitable host for photoluminescence applications [49–51]. Doped and undoped lanthanide nickelates shows giant/colossal dielectric properties [52–54].

In the last several years, rapid growth in solar cells and optoelectronic devices based on 3D organic-inorganic halide-based perovskites is observed. But due to their inherent instabilities over moisture, light and heat strongly hindered this growth. Recently 2D organic-inorganic based layered perovskites received increasing attention owing to their superior ambient stability. These 2D perovskites have demonstrated to exhibit abundant and tunable optoelectronic properties, high quantum efficiency, and large specific surface area, which hold a good prospect for a range of electronic and optical applications [55,56].

During 1980-1990, C. N. Rao and his group carried extensive research work on structure and magnetic properties of A_2BO_4 oxides [57,58]. Magnetic properties of these oxides were investigated more extensively than transport properties. They published a few review articles and chapters in the book on these oxides [59]. After observation of superconductivity up to 35 K in the Ba-doped La_2CuO_4 ternary compound by Alex Mueller and George Bednorz of IBM Zurich Laboratory in 1986 [60], research works on A_2BO_4 oxides further intensified. However, in the last two decades, these oxides have attracted attention because of their applications based on their electrical, optical and dielectric properties.

1.2.1 Crystal Structure

The A_2BO_4 compounds crystallize in two major structural forms: T-type and T′-type [61]. The schematic structure of T-type La_2NiO_4 ternary oxide is shown in Fig. 1.4(a). For clarity, only half cell ($a/2 \times b/2 \times c$) is shown. The Ni cations are located at the center of apically elongated octahedra, also known as NiO_6 octahedra; the six $Ni-O$ distances are: $Ni-O_{bs}(O(1)) \times 4 = 1.947$ and $Ni-O_{ap}(O(2)) \times 2 = 2.267$ Å, two long distant atoms are along the c-axis. The La cation is surrounded by nine oxygen atoms, four O_{ap} atoms (in the same level of La atom), four O_{bs} atoms (in Ni level, above (below)) and one O_{ap} atom (head-below (head-above) from La atom). These nine O atoms make a LaO_9 polyhedra. The La atom is not located at the center of this polyhedra, but it is little shifted towards the capping O_{ap}. The NiO_6 octahedra and LaO_9 polyhedra shares faces with each other and each NiO_6 octahedra is connected with four nearest neighboring NiO_6 octahedra in ab-plane by common shared O_{bs} atoms. Each NiO_6 octahedra with eight La atoms of O_{ap} level makes an $LaNiO_3$ perovskite unit. Between two perovskite units, there is an LaO rocksalt layer in ab-plane. Therefore, the La_2NiO_4 structure can be described as an intergrowth of an alternative layer of $LaNiO_3$ perovskite and LaO rocksalt along the c-axis. Thus T-type A_2BO_4 ternary oxides are known as A_2BO_4 layered perovskite or RP-phase layered perovskite. K_2NiF_4 has a similar structure. Hence, this structure is also commonly referred as K_2NiF_4 structure.

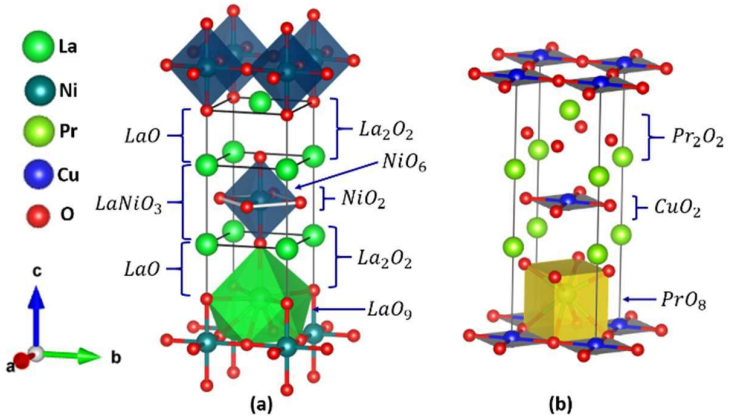

Figure 1.4. (a) Half unit cell of T-type La_2NiO_4 layered perovskite. (b) Unit cell of T′-type Pr_2CuO_4 ternary oxide.

In contrast to T-type structure in T′-type structure, the cationic arrangement is the same, but the anionic arrangement is different [62]. Basal oxygens, O_{bs}, do not change its position but apical oxygens, O_{ap}, are shifted to the face of the unit cell, between the levels of cation A, designated as O_f. The schematic structure of T′-type Pr_2CuO_4 ternary oxide is shown in Fig. 1.4(b). The Cu cation is surrounded by four O_{bs} atoms and their interionic distances are 1.98 Å. The Pr cations are surrounded by eight O atoms: four O_{bs} atoms are in the Cu level and four O_f are between the level of Pr atoms, makes an PrO_8 cube.

The A_2BO_4 compounds can also be visualized as alternative stacking of BO_2 and A_2O_2 bilayers along c-axis [63]. In La_2NiO_4, four halves shared (between unit cells) O_{bs} atoms and one Ni atom makes NiO_2 layer, similarly two O_{ap} and two La atoms make La_2O_2 bilayer, as shown in Fig. 1.4(a), so the structure of La_2NiO_4 compromises the following sequences of layers.

$$(NiO_{bs})_o(LaO_{ap})_c(LaO_{ap})_o(NiO_{bs})_c(LaO_{ap})_o(LaO_{ap})_c(NiO_{bs})_o \ldots.$$

The subscript o and c indicate whether the cation is at the origin or center of the mesh, respectively. Similar stacking of BO_2 and A_2O_2 bilayers in T′-type structured Pr_2CuO_4 is also

schematically shown in Fig. 1.4(b). The A_2BO_4 compounds also crystalize in T*-type of structure, which is a hybrid of T- and T′-type structure [61]. Recently several research groups have investigated the T- and T′-type structures using well known **Goldschmidt tolerance factor t as a criterion**. The tolerance factor is based on the analysis of perovskite supercells (also known as perovskite tolerance factor) and given as follows [64]:

$$t = \frac{r_A + r_O}{\sqrt{2(r_B + r_O)}} \qquad (1.2)$$

where, r_A, r_B and r_O are ionic radii of cation A, cation B, and oxygen, respectively. The tolerance factor 't' for T- type structure is found in the range of $0.99 \geq t \geq 0.87$ while for T'-type structure the tolerance factor lies in the range of $0.86 > t \geq 0.83$. Under high pressure, the lower limit of t for T′-type structure extends upto 0.81. The T*-type structure exists for a narrow range of tolerance factors, lies in between the t of T- and T'-type structure [61].

Most of the A_2BO_4 layered perovskites crystallize either in orthorhombic structure or in tetragonal structure. The tolerance factor t for tetragonal and orthorhombic structure lies in the range of $0.99 \geq t \geq 0.88$ and $0.88 \geq t \geq 0.865$, respectively [63]. The A_2BO_4 layered perovskites can be further subdivided in two groups, one which consist rare earth element (RE = La, Nd, Pr, etc.) as cation 'A' and another which consists alkali earth element (AE = Ca, Sr, Ba) as cation 'A'. The layered perovskites consisting RE as cation 'A', consists transition metal(s) (M = Ni, Cu, Co, etc.) in divalent state as cation 'B' and the other group which consist AE as cation 'A', consists of transition element(s) or post-transition element(s) (M′ = Mn, Sn, Ti, etc.) in the tetravalent state, as cation 'B'. These two groups of layered perovskites can be named as RE_2MO_4, and $AE_2M'O_4$, respectively. In recent years another group of A_2BO_4 layered perovskites or doped A_2BO_4 layered perovskites are also studied, which consist of both rare earth and alkaline earth elements in the form of cation 'A' and cation 'A'' in equal or

unequal stoichiometries. The general structural formula for this group of compounds is sometimes written as '$A_xA'_{2-x}BO_4$'. Majority of RE_2MO_4, crystallize in orthorhombic structure with space group $Bmab, P4_2/ncm, Pccn, etc.$ while $AE_2M'O_4$ crystallize in tetragonal structure with space group $I4/mmm, P4/mmm, etc.$.

1.2.2 Oxygen Stoichiometry and Carrier Concentration

The A_2BO_4 layered perovskites are generally synthesized via solid-state reaction method. During high-temperature synthesis processes ($>$ 1000 °C), excess oxygens may accommodate in the structure at the interstitial sites and/or oxygen vacancies are created in the structure. These excess oxygens in the structure are accommodated in the form of doubly ionized oxide ions, O_i^{2-}. In this thesis, Kröger-Vink notation has been followed to represent charge species and defects. In Kröger-Vink notation, the positively charged species are marked as '•' in superscript. Similarly, the negatively charged species are marked as '′' in superscript. When an oxide ion, O_i'' accommodates the interstitial sites, two excess holes, $h^{\bullet}$ are created in the structure. Similarly, when an oxygen vacancy, $V_o^{\bullet\bullet}$ is created two excess electrons, e' are created in the structure. Generation of these defects are represented by Eqns. (1.3) and (1.4) [65].

$$\frac{1}{2}O_2(g) = O_i'' + 2h^{\bullet} \qquad (1.3)$$

$$O_o^{\times} = V_o^{\bullet\bullet} + \frac{1}{2}O_2(g) + 2e' \qquad (1.4)$$

These excess holes may recombine with electrons or with divalent transition metal ions according to Eqns. (1.5) and (1.6), respectively;

$$h^{\bullet} + e' = 0 \qquad (1.5)$$

$$M^{2+} + h^{\bullet} = M^{3+} \qquad (1.6)$$

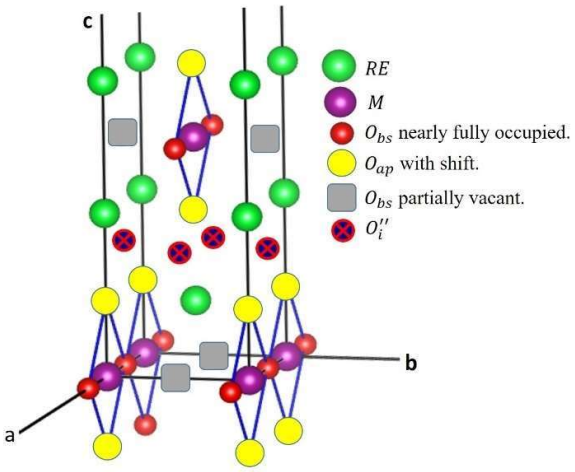

Figure 1.5. Schematic representation of location of oxygen vacancies and interstitial oxide ions in A_2BO_4 layered perovskite [66].

In RE_2MO_4, RE_2O_2 bilayer is electropositive and MO_2 layer is electronegative. Excess oxide ions mostly accommodate in the RE_2O_2 bilayer interstitials and holes generally go in the MO_2 layer due to their electropositive and electronegative nature, respectively. By this mechanism, excess oxide ions in the structure facilitate in neutralizing the electronic polarity of layers. It is also repoted that in RE_2MO_4 oxides, excess oxide ions at interstitial sites minimize the electronic polarity between the RE_2O_2 and MO_2 intergrown layers [66,67]. There are also reports on RE_2MO_4, in which the creation of oxygen vacancies at basal oxygen sites, i.e., in MO_2 layers is discussed [68]. The electronic polarity of intergrown RE_2O_2 and MO_2 layers, inhibits the creation of oxygen vacancy in RE_2O_2 bilayer [67]. Location of oxygen vacancy and interstitial oxygen is schematically shown in Fig. 1.5 [67]. The oxygen stoichiometry of RE_2MO_4 depends on the number of excess oxide ions at interstitial sites and

number of oxygen vacancies in the structure. The interstitial oxide ions O_i'', in RE_2O_2 bilayers play crucial role in reducing the stresses produced by the above-mentioned mismatch of interionic distances of $RE-O_{ap}$ and $M-O_{bs}$ [67]. On the accommodation of oxygen at interstitial sites, the electrostatic repulsion between O_i'' and neighboring apical oxygen O_{ap} of RE_2O_2 bilayer increases the lattice parameters 'a'and 'c' which facilitates to release of compressive and tensile stresses present in MO_2 layer and RE_2O_2 bilayer, respectively. It is also known that ionic radii of transition metal ions in lower oxidation state is smaller than their higher oxidation state. Hence, oxidation of transition metal ions reduces the effective interionic distances of $M-O_{bs}$. Due to these two processes taking place simultaneously majority of RE_2MO_4 oxides exbibit a structural transformation with increasing concentration of interstitial oxide ions [69–71]. For e.g., the hyper-stoichiometric (oxygen excess) $La_2NiO_{4+\delta}$ $(0.10 < \delta < 0.15)$ transforms from orthorhombic to tetragonal phase [72]. The A_2BO_4 layered perovskites also exhibit a structural transformation on becoming hypo-stoichiometric (oxygen deficient). For example, when Sr_2MnO_4 becomes hypo-stoichiometric, i.e., $Sr_2MnO_{3.5}$, transform from tetragonal to monoclinic phase [73,74].

The oxygen stoichiometry and carrier concentration in structure can also be tailored by substitutions at A and B sites. There are three kinds of substitutions (isovalent, donor, and acceptor) have been done in A_2BO_4 layered perovskites. Further, in case of isovalent substitution, substituted ion may have smaller or larger ionic radius than the host ion. Isovalent substitution of smaller ionic radii helps in increasing the void space of interstitial sites, thus, supports accommodation of higher concentration of excess oxygen in the structure. The substitution of larger ionic radii has vice versa effect. The isovalent substitution also helps in increasing or reducing the above-mentioned stresses of intergrown layers, due to increment or decrement in interionic distances, respectively. For example, on substitution of Ni in

$La_2Cu_{1-x}Ni_xO_{4+\delta}$ oxygen content increases with the increasing content of Ni. The size of octahedra with Ni get reduced due to the smaller ionic radius of Ni ($r_{Ni^{2+}} = 0.69$ Å) as compared to Cu ($r_{Cu^{2+}} = 0.73$ Å). Thus, void space in La_2O_2 bilayer is increased and facilitates easier accommodation of O_i'' [69].

The donor substitutions are generally done in $AE_2M'O_4$ by substituting RE ions at the AE site. The RE substitution creates excess electrons in the structure according to Eqn. (1.7). These excess electrons may reduce M'^{4+}cation to M'^{3+}, according to Eqn. (1.8). On account of this, the $RE_xAE_{2-x}O_2$ rocksalt bilayer becomes electropositive and $M'^{3+}_yM'^{4+}_{1-y}O_2$ becomes electronegative, which helps in accommodating more O_i'' in $RE_xAE_{2-x}O_2$ rocksalt bilayers. For example, $La_xSr_{2-x}MnO_{4+\delta}$, $(0.25 \leq x \leq 0.6)$ consist of excess oxygen in the structure as compared to Sr_2MnO_4 [48]. Excess electrons created due to RE substitution does not only reduce M' cations, but also some of them may recombine with excess holes (according to Eqn. (1.5)) created by interstitial oxide ions (according to Eqn. (1.3)). If these two processes of reduction of M'^{4+} cation and recombination of electron and hole occurring simultaneously (may make $x \neq y$), the concentration of reduced M' ion can be different from twice of concentration of RE substituent.

$$RE_2O_3 = 2(RE^{3+}_{AE^{2+}})^{\bullet} + 2O_o^{*} + \frac{1}{2}O_2(g) + 2e' \qquad (1.7)$$

$$(M'^{4+}_{M'^{4+}})^{\times} + e' = (M'^{3+}_{M'^{4+}})' \qquad (1.8)$$

The acceptor substitutions in RE_2MO_4 have been made by replacing RE ions with AE ions. Acceptor dopants normally create excess holes in the structure according to Eqn. (1.9). These excess holes recombine with neutral oxygen vacancies and help them stabilizing as $V_o^{\bullet\bullet}$, according to Eqn. (1.10). Another possibility is that these excess holes recombine with divalent (M^{2+}) ions to form trivalent ions (M^{3+}) as given by Eqn. (1.11).

$$AEO = \left(AE_{RE^{3+}}^{2+}\right)' + \frac{1}{2}O_2(g) + h^{\bullet} \quad (1.9)$$

$$V_O^{\times} + 2h^{\bullet} = V_O^{\bullet\bullet} \quad (1.10)$$

$$(M_{M^{2+}}^{2+})^{\times} + h^{\bullet} = (M_{M^{2+}}^{3+})^{\bullet} \quad (1.11)$$

1.2.3 Electrical Properties

In the beginning of twentieth century $A_2BO_{4\pm\delta}$ layered perovskites renewed their interest after the investigation of oxygen transport properties of $La_2NiO_{4\pm\delta}$ at high temperature [75–77]. Electrical properties of $A_2BO_{4\pm\delta}$ layered perovskites at low temperature were extensively studied after the discovery of superconductivity in $La_2CuO_{4\pm\delta}$. But in recent years, more attention has been focused on the study of high-temperature electronic and oxide ion transport properties of $A_2BO_{4\pm\delta}$ layered perovskites. In this context, $La_2NiO_{4\pm\delta}$ is widely studied for their phase stability, oxygen stoichiometryand high-temperature transport properties, and a comparative study with $La_2CuO_{4\pm\delta}$ is established. $La_2NiO_{4\pm\delta}$ shows a semiconductor to metal-like transition at $350\,°C$ and have electrical conductivity $100\ \Omega^{-1}cm^{-1}$ at transition temperature which is lower than electrical conductivity of mixed electronic-ionic conducting perovskite oxides [78]. However, oxide ion conductivity of $La_2NiO_{4\pm\delta}$ in the intermediate temperature range is higher than that of mixed electronic-ionic conducting perovskite oxides. Skinner et al. have shown that oxide ion conductivity is higher in $La_2NiO_{4+\delta}$ than conductivity of $La_{0.6}Sr_{0.4}Co_{0.2}Fe_{0.8}O_3$ (LSCF), but, one order lower than the best perovskite oxide ion conductor $La_{0.3}Sr_{0.7}CoO_3$ (LSC) perovskite [79]. Most of the undoped A_2BO_4 layered perovskites are poor oxide ion conductor due to less oxygen vacancies and interstitial oxide ions [80]. As discussed above, on partial substitution the oxygen stoichiometry tunes, i.e. material either becomes hypo-stoichiometric or hyper-stoichiometric [48,81]. Oxygen vacancies in the structure provide necessary pathways for oxide ion migration

via hopping through the vacant sites [82]. Generally, on acceptor substitution A_2BO_4 layered perovskites becomes hypo-stoichiometric. But, sometimes even after substituting acceptor ions structure is hyper-stoichiometric. This is because of excess number of interstitial oxide ions than the oxygen vacancies in structure. The interstitial oxide ions also migrate in the structure and contribute to the oxide ion conductivity. Some of acceptor substituted hyper-stoichiometric structures show high mixed ionic and electronic conductivity [79]. The substitution of acceptor cations at A-site also promotes the oxidation of B-cation, according to Eqn. (1.11). Partial oxidation of B-cation enhances the electrical conductivity. Electron bounded with unoxidized B-cation hops to neighboring oxidized B-cation. During this hopping process, the unoxidized B-cation oxidizes and oxidized B-cation reduces and become unoxidized. Similarly, hole bounded with oxidized B-cation hops to neighboring unoxidized B-cation, and during this hopping process, the oxidized B-cation reduces and unoxidized B-cation oxidizes. Sometimes these hopping processes, also produces a lattice distortion on local level at reducing and oxidizing B-cation sites, due to Jahn-Teller (JT) effect [48,83,84]. Thus, the hopping of electron/hole between the reduced and unreduced B-cation is different from the conduction of electron in metals and conduction of electron/hole in semiconductors. In some materials, local lattice distortion and electron/hole make a bound pair with each other (known as polaron), and conduction of these bound pair is known as polaronic conduction [28,85,86]. Further, when two polarons get closer and bound with each other to minimize their energy by sharing distortion with each other is known as bound bipolaron. Strongly bounded bipolarons are small in size and have integer spin. Thus, have bosonic properties. Formation of bipolarons without sharing distortion with each other is possible by Bose-Einstein condensation mechanism. This might be a possible mechanism for high-temperature superconductivity. The theme of this thesis work makes this discussion out of the scope of this thesis.

1.2.4 Applications

The discovery of superconductivity in the $La_{2-x}Ba_xCuO_4$ system was derived from the La_2CuO_4, has added additional dimension in the investigation of these phases [72,73]. However, there was a great deal of interest in the physical and structural chemistry of perovskite - related compounds for their wide range of applications, such as ideal semiconductors, magnetic materials, high temperature superconductors, catalysts, electrode materials etc. even before the discovery of superconductivity [81, 82]. The properties of $La_2CuO_{4+\delta}$ are extremely sensitive to change in oxygen stoichiometry. An antiferromagnetic and semiconductor behaviour is shown by a negative value of δ in $La_2CuO_{4+\delta}$. However, antiferromagnetism disappears with change in oxygen stoichiometry as small as 1%. As δ becomes positive, the holes are introduced into the structure and metallic behaviour is observed [87]. When La_2CuO_4 is doped with holes either by introducing excess oxygen into the structure or partial replacement of La by alkaline earth metal ions, then it oxidized the mixed valent state of Cu from Cu^{2+} to Cu^{3+} and responsible for showing superconductivity [87].

Anion related non stoichiometric is also very common in perovskite and related compounds. Low concentrations of oxygen vacancies or interstials in perovskite type oxide are often disordered and results in potential applications of material as ionic or mixed ionic electronic conductors (MIECs). However, the higher degree of oxygen deficiency results p-type semiconductor behaviour in ordered structures and improves their hole conductivity. The doped and undoped La_2NiO_4 is one of the widely studied systems. The crystal structure of La_2NiO_4 is reported to be tetragonal with space group $I4/mmm$. However, X-ray diffraction (XRD) studies indicate a monoclinic distortion. La_2NiO_4 exhibits a semiconductor to metal transition around 550 K, while $La_{2-x}Sr_xNiO_4$ is reported to be exhibit a superconducting state down to 70 K [58]. La_2NiO_4 annealed in CO_2 atmosphere at 1400 K, show evidence for long

range antiferromagnetic ordering. $La_2NiO_{4+\delta}$ also exhibits mixed electronic and ionic conductivity which makes it useful for cathodes in IT-SOFCs, ceramic membranes for oxygen separation. The value of thermal expansion coefficients (TEC) ≈ 13.0x10^{-6} K^{-1} for $La_2NiO_{4+\delta}$ was close to the TEC of conventional materials which are widely used as electrolytes in SOFC like $Zr_{0.92}Y_{0.08}O_{2-y}$ (YSZ), and $Ce_{0.9}Gd_{0.1}O_{2-y}$ (CGO). This is the possible reason which makes these materials more popular than other oxides and perovskite oxides [90]. The similar TECs values guarantee the thermo-mechanical compatibility between cell components. In their crystalline structure accommodation of interstitial oxygen promotes the ionic conductivity [91], and the p-type electronic conductivity [92]. Although, the value of oxygen non-stoichiometric of layered perovskite (RP phases) playing a key role in the improvement of the electronic and ionic conductivity. Most of these compounds, showing interesting electric transport and magnetic properties, crystallizes either in tetragonal or orthorhombic crystal symmetry in the space group $I4/mmm$, $Fmmm$ or $Cmca$ [87–90].

Recently, some of A_2BO_4 oxides having giant/colossal dielectric constant were explored. Doped and undoped La_2NiO_4 show very large (‘Giant”) magnitude of the dielectric constant and thus displays immense potential for their applications in modern microelectronics and for the development of capacitor-based energy storage devices. The dielectric properties of $La_{15/8}Sr_{1/8}NiO_4$ are superior than popular high dielectric constant material $CaCu_3Ti_4O_{12}$ (CCTO). Until now no ferroelectric characteristics have been observed experimentally in any A_2BO_4 layered perovskites. Theoretical researchers have suggested certain compositional and structural modifications to induce highly improper ferroelectricity (HIF) in RP oxides.

In the last decade researchers have mainly focused attention on La_2NiO_4, studies on the properties of other oxides such as A_2BO_4 ($A = Ca, Sr, Ba$ and $B = Sn, Ti, Mn$) are very limited. The studies of these other A_2BO_4 oxides are essential to explore the hidden potential of them.

1.3 Permittivity (ε) and Permeability (μ)

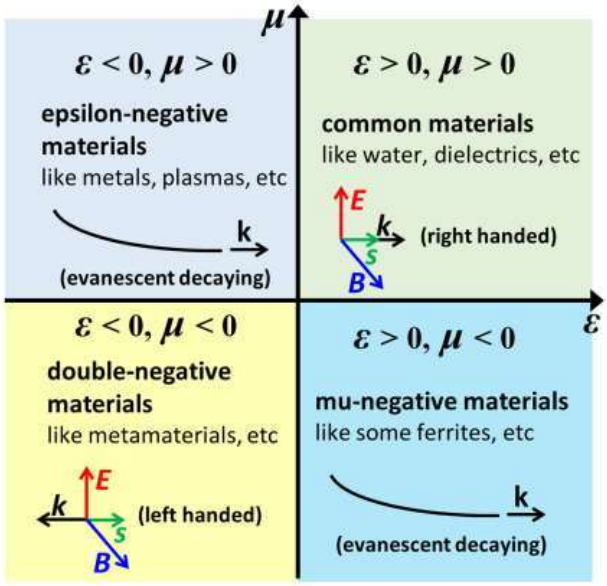

Figure 1.6. Classification of materials according to their permittivity (ε) and permeability (μ) [96].

Permittivity and permeability are two fundamental physical properties of materials that describe how they react to electric, magnetic, and electromagnetic forces [97–99]. Materials are divided into four quadrants based on the sign of permittivity and permeability, as illustrated in Fig. 1.6 [100–102]. These quadrants include common materials, double-negative materials, negative permeability materials, and negative permittivity materials. The incident electromagnetic waves are transparent to common materials with positive permittivity and permeability, and the electric vector (**E**), magnetic vector (**B**), and wave vector (**k**) correspond to the right-handed rule. Electromagnetic waves can propagate within materials having double negative characteristics, such as metamaterials, but the relationships between **E**, **B**, and **k** are left-handed. In materials with solely negative permittivity or negative permeability, electromagnetic waves fade evanescently. Negative permittivity was initially realised in metamaterials, while negative permeability characteristics were first obtained in ferrites at their magnetic resonance frequency. The negative electromagnetic characteristics, such as negative

permittivity and negative permeability, have recently become a hotspot in materials science research, and these studies are essential additions to materials research.

1.4 Negative Permittivity Materials

Negative permittivity has attracted widespread attention in the optical dielectric function of metals and semiconductors [103,104]. Negative permittivity is required in metamaterials for meta-performances such as negative refraction, negative phase velocity, reverse Doppler effect, and Cerenkov effect, and others [105–107]. The negative permittivity is very common in metals below their plasmonic frequency, ω_p. The plasmonic frequency (ω_p) of common metals is usually in optical frequency. With frequency decreasing, the real part of permittivity decreases rapidly and simultaneously the imaginary part increases dramatically. According to investigations conducted from the standpoint of materials science the negative permittivity can be realised in the radio-frequency band, which is significantly lower than the optical frequency [108–110]. As mentioned above, the negative permittivity was initially realised in metamaterials. Later few composites were investigated/studied to realize negative permittivity. The negative permittivity materials composed out of composites are classified as meta-composites, which are the composites that have novel and distinctive features that set them apart from other materials [111–113]. Thus, negative permittivity materials can be classed as metamaterials or meta-composites. The meta-composites are being separated into ceramic matrix composites and polymer matrix composites based on their composition. The negative permittivity materials can also be made up of homogenous ceramics or doped polymers. The negative permittivity materials have also showed promises in a variety of electromagnetic and electronic applications, including electromagnetic shielding, wave absorption, laminated capacitors, and coil-less inductors [114–117].

1.4.1 Metamaterials

Metamaterials are artificial materials made out of periodic building blocks that have a number of unique physical features not found in natural materials [118,119]. Metamaterials creation techniques can be used to create new types of electromagnetic medium with anomalous negative physical properties. To produce negative electromagnetic properties, periodic metallic unit arrays are required [120]. The realization and regulation of the performance of metamaterials are dependent on the excogitation of the geometries and configurations of the building blocks, which is almost independent on the composition of the components. Here it is important to mention here that these unique electromatic properties of metamaterials are designed artificially rather than being determined by the materials' composition and microstructure. Metamaterials with the right design can alter electromagnetic waves in ways that aren't seen in bulk materials [101]. Those that exhibit a negative index of refraction for particular wavelengths have been the subject of extensive research. These materials are named as negative-index metamaterials

Optical filters, medical devices, remote aerospace applications, sensor detection and infrastructure monitoring, smart solar power management, crowd control, radomes, high-frequency battlefield communication and lenses for high-gain antennas, improving ultrasonic sensors, and even shielding structures from earthquakes are some of the potential applications of metamaterials [121–124]. Metamaterials could be used to make super-lenses [103]. Such a lens can allow imaging below the diffraction limit, i.e., the minimum resolution $d = \lambda/(2NA)$ that can be achieved by conventional lenses having a numerical aperture NA and with illumination wavelength λ. Sub-wavelength optical metamaterials when used with optical recording media, it can attain optical data densities greater than those limited by diffraction

[125]. Gradient-index metamaterials were used to realise a form of 'invisibility.' Metamaterials for acoustic and seismic applications are also in study. [126,127].

In 1968, V. G. Veselago firstly envisaged the substances with simultaneous negative permittivity and negative permeability, and expounded the rule of propagation for electromagnetic wave in media with negative electromagnetic parameters [106]. Until 1996, J. B. Pendry proposed metallic mesostructures made of thin metal wires to achieve negative permittivity in GHz bands [102]. In fact, under the influence of electromagnetic waves, metals show plasma characteristics, and the frequency dependence of permittivity is stated as [100]:

$$\varepsilon = 1 - \frac{\omega_p^2}{\omega^2 + i\omega\gamma} \qquad (1.12)$$

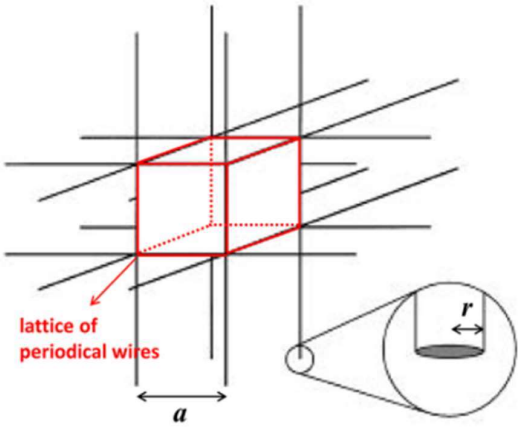

Figure 1.7. Schematic diagram of lattice of periodic metal wires proposed by J. B. Pendry [96].

The plasma frequency is defined by the effective electron concentration (n_{eff}) and effective mass (m_{eff}) of electrons, where ω_p is the plasma frequency and γis a damping factor that represents the energy dissipation in a system. Because γ is substantially smaller than ω_p for simple metals, it may be assumed that the sign of permittivity is mostly governed by plasma frequency, which is given by $\omega_p = \sqrt{\frac{n_{eff}e^2}{m_{eff}\varepsilon_0}}$. The permittivity of common metals is always negative when the frequency is below ω_p, i.e., all metals below their plasma frequency are

ENMs on their own. However, as frequency falls, the real part of permittivity rapidly declines while the imaginary part substantially increases. As a result, all metals lose their utility as ENMs in various applications.

The realization of negative permittivity in the GHz band in Pendry's work is based on an array structure of thin metal wires. As shown in Fig. 1.7, if thin metal wires with a diameter of $d = 2r$ (r =radius of wire) are arranged into cubic structures and the distance between two wires is a, the effective average concentration (n_{eff}) of this cubic lattice can be calculated as follows:

$$n_{eff} = \frac{\pi r^2 n}{a^2} \qquad (1.13)$$

where, n is the electron concentration in metal wires. Meanwhile, affected by the self-inductance of the wire structure, m_{eff} of electrons in the wire arraysis expressed as:

$$m_{eff} = \frac{\mu_0 \pi r^2 e^2 n}{2\pi} \ln\frac{a}{r} \qquad (1.14)$$

Therefore, ω_p of the metal wire array is:

$$\omega_p = \frac{2\pi\mu_0\varepsilon_0}{a^2 \ln(a/r)} \qquad (1.15)$$

This is being determined from the metal wires' configuration, thickness, and electron concentration. As a result, the plasma frequency could be transferred to the microwave band, which is much lower than ultraviolet, and the negative permittivity could be easily controlled by modulating the wire arrays [102].

1.4.2 Composites

According to materials science, a material's physical properties must be determined by its composition and microstructure, which explains material structure-activity relationships and

enables researchers to improve material properties by changing the composition and microstructure of constitutive components [121,122]. So, can the "real" materials acquire metamaterial's kind features like negative permittivity and/or negative permeability? At the beginning of metamaterials research, only a few materials studies focused on whether conventional materials have the unique properties of metamaterials. The composites with the advantage of integrating multi-component properties provided a convenient method to achieve negative electromagnetic parameters [123,124]. The meta-performance of composite materials was realised and customised using traditional materials preparation procedures that modulate chemical compositions and their microstructures.

Negative permittivity can be achieved in different frequency bands by changing the plasma frequency, according to Eqn. (1.12). Which is principally determined by $\omega_p = \sqrt{\frac{n_{eff}e^2}{m_{eff}\varepsilon_0}}$, i.e., effective carrier concentration and effective mass of charge carriers. The dilution of electron concentration, i.e., the dilution of effective carrier concentration, was the sole reason for constructing mesostructures of thin metal wire in metamaterials. Other methods of dilution of effective carrier concentration can also be used. As a result, there are two types of composites that have been thoroughly studied and investigated by various research groups. These composites are:

A. Ceramic matrix composites (CMCs), and
B. Polymer matrix composites (PMCs)

1.4.2.1 Ceramic matrix composites (CMCs)

Composites are made up from two or more separate components, that have novel properties, are very distinct from the individual components' properties [122,128]. The principles of composites preparation made it easier to create and realise a variety of innovative

features that are rarely encountered in basic substances. As a result, a wide range of adaptable composites with enhanced physical/chemical properties have been produced and are widely employed in electrical, magnetic, acoustic, optical, thermal, and other applications or devices [129,130]. CMCs are composites that use ceramics as the matrix and conducting materials as fillers, which poses advantages like the high hardness, strength, and high wear resistance of ceramics. In the field of dielectrics, CMCs with metal fillers and a high dielectric constant matrix have gotten a lot of attention [131]. Copper (Cu), nickel (Ni), and even molybdenum (Mo) have been incorporated into dielectric ceramic (such as BaTiO3) matrix to raise the dielectric constant of the composites, which is critical for the development of high dielectric constant materials [132–134]. When the metal content of metal/ceramic composites is below the percolation threshold, the dielectric constant increases, and when the filler content exceeds the percolation threshold, the dielectric constant turns into negative value [135,136]. The percolated CMCs with the metal content beyond percolation threshold have been verified to be ENMs in the radiofrequency band, and the negative permittivity is intimately associated with the composition and microstructure of CMCs. The metal fillers gradually become interconnected and eventually form networks within the ceramic matrix when the metal content rises over the percolation threshold. The mesostructure of thin metal wires in metamaterials is remarkably similar to the network of interconnected metal fillers. As a result, the dilution of the electron concentration, i.e., the dilution of effective carrier concentration, is achieved in a similar manner above the percolation threshold. As a result, the electric and dielectric characteristics change dramatically over the percolation threshold. The electric conductivity improves as the metal concentration rises, and the dielectric permittivity shifts from positive to negative as the interconnected metallic networks take shape. Metal fillers can have varieties of shapes and sizes, including particles, particle clusters, networks, and flower-like flakes. As a result, a more diverse microstructure design for metal/ceramic composites is possible, and the

negative permittivity properties of the composites are confirmed to be influenced by the composition and microstructure. Researchers in this field have produced examples for preparing negative permittivity materials with composites, which has aided in the electromagnetic functionalization of traditional structural cermets.

Multiphase ceramics, in addition to metal/ceramic composites, are a type of composite that can achieve negative permittivity characteristics. To manufacture the ceramic composites, one kind combines conducting ceramics (such as TiN and TiC) and insulating ceramics (such as Al_2O_3), while the other uses $BaTiO_3$, $SrTiO_3$, $BiFeO_3$, and other ferroelectric materials as functional fillers [137–141]. The difference is that the former is akin to metal/ceramic composites with plasma-like negative permittivity behaviour, whereas the latter's negative permittivity behaviour is mostly produced by dielectric resonance. Negative permittivity out of plasma-like behaviour are across a wide frequency range below the plasma frequency, whereas resonance-type negative permittivity has negative values primarily around the resonant frequency. Negative permittivity is attributed to plasma oscillations of free electrons in metal/ceramic composites, but no free electrons are involved in ferroelectric ceramic composites, and the ensuing negative permittivity performance is caused by dipole resonance under the action of an electric field. The frequency band and the strength of the resonance in these ceramic composites are also impacted by composition, which can be controlled to achieve negative permittivity in a certain frequency range [138,142].

1.4.2.2 Polymer matrix composites (PMCs)

PMCs are composites having a polymer matrix and carbonaceous materials, polymers, metals, and ceramics as functional fillers [143–145]. Negative permittivity can be achieved in PMCs, just like it can in CMCs, with enough conductive fillers. Polymer materials as a matrix could make PMCs more flexible and elastic than ceramic matrix [145]. Sun et al. used a simple

tape casting approach to make MWCNTs/PDMS composites [145]. Negative permittivity is detected in composites with only 5 wt. % MWCNTs due to the large aspect ratio of MWCNTs very low percolation threshold is very low, and graphene as fillers also causes negative permittivity in PDMS composites at very low filling content [146]. The filling of graphene or conductive carbon fibres ensures the composites show out negative permittivity properties [147,148]. A more convenient process of mixing and curing was used to prepare PVA matrix composites, and the filling of graphene or conductive carbon fibres ensures the composites show out negative permittivity properties. Despite the incorporation of carbonaceous fillers, composites made of PDMS or PVA are flexible and stretchable, suggesting that polymer matrix-ENMs could be used in some wearable devices. Negative permittivity PMCs provide greater design options. The elastic deformation of the polymer matrix altered the negative permittivity properties realised with Ag-nanowires/polyurethane sponge, implying that compressible ENMs might be employed as deformation sensors by measuring the variation of negative permittivity versus applied external force [149]. PMCs' negative permittivity properties has been demonstrated in the kHz, MHz, and GHz frequency ranges, and negative permittivity polymer composites are progressively emerging as a new branch of negative permittivity metamaterials [150–152].

1.5 Theoretical Models

When a material is exposed under the varying electric field, the free and bound charge carrier of materials behaves differently. A theoretical model was proposed to study the behaviour of free electron of material under varying electric filed Paul Drude in 1900 [153,154]. Further, this theoretical model was extended by Hendrik Antoon Lorentz in 1905 for studying behaviour of bound charge carriers under varying electric field [155–157]. Thus,

combinedly known as Drude-Lorentz Oscillator model or simply, Drude-Lorentz model. Both models are described below explicitly, further these are combined at end.

1.5.1 Drude Model

The momentum ($\mathbf{p}$) of electron in time-dependent electric field ($\mathbf{E} = \mathbf{E_0}\, e^{-i\omega t}$) with an angular frequency ω can be written as:

$$\frac{d}{dt}\mathbf{p}(t) = -e\mathbf{E} + \frac{\mathbf{p}(t)}{\tau}$$

where, τ is relaxation time of electron's collision. The possible solution of this equation of motion can be $\mathbf{p}(t) = \mathbf{p_0}\, e^{-i\omega t}$, substituting,

$$-i\omega\mathbf{p_0} = -\frac{\mathbf{p_0}}{\tau} - e\mathbf{E_0}$$

Hence,

$$\mathbf{J} = -ne\frac{\mathbf{p}}{m} = \frac{\sigma_0}{1 - i\omega\tau}\mathbf{E} = \sigma^*(\omega)\mathbf{E}$$

Thus, The AC conductivity $\sigma^*(\omega) = \frac{\sigma_0}{1-i\omega\tau} = \frac{\sigma_0}{1+\omega^2\tau^2} + i\frac{\sigma_0\omega\tau}{1+\omega^2\tau^2};\ \sigma_0 = \frac{ne^2\tau}{m}$

The Maxwell's equations are:

$$\nabla.\mathbf{E} = 0;\ \nabla.\mathbf{B} = 0;\ \nabla\times\mathbf{E} = -\frac{\partial\mathbf{B}}{\partial t};\ \nabla\times\mathbf{B} = \mu_0\mathbf{J} + \mu_0\varepsilon_0\frac{\partial\mathbf{E}}{\partial t}$$

$$\nabla\times(\nabla\times\mathbf{E}) = -\frac{\partial}{\partial t}(\nabla\times\mathbf{B}) = -\frac{\partial}{\partial t}\left(\mu_0\mathbf{J} + \mu_0\varepsilon_0\frac{\partial\mathbf{E}}{\partial t}\right) = -\frac{\partial}{\partial t}\left(\mu_0\sigma^*\mathbf{E} + \mu_0\varepsilon_0\frac{\partial\mathbf{E}}{\partial t}\right)$$

The possible solution is $\mathbf{E} = \mathbf{E_0}\, e^{-i\omega t}$, substituting,

$$\nabla^2\mathbf{E} + \frac{\omega^2}{c^2}\left(1 + \frac{i\sigma^*}{\omega\varepsilon_0}\right)\mathbf{E} = 0$$

Can be written as,

$$\nabla^2\mathbf{E} + \frac{\omega^2}{c^2}\varepsilon_r^*(\omega)\mathbf{E} = 0$$

where, $\varepsilon_r^*(\omega) = 1 + \frac{i\sigma^*}{\omega\varepsilon_0}$ is the complex dielectric constant.

$$\varepsilon_r^*(\omega) = 1 + \frac{i\sigma^*}{\omega\varepsilon_0} = 1 + \frac{i}{\omega\varepsilon_0}\left(\frac{\sigma_0}{1 - i\omega\tau}\right) = 1 - \frac{\omega_p^2}{\omega^2 + i\omega\gamma}$$

$$\varepsilon_r^*(\omega) = \left(1 - \frac{\omega_p^2}{\omega^2 + \gamma^2}\right) + i\left(\frac{\omega_p^2\gamma}{\omega(\omega^2 + \gamma^2)}\right) \qquad (1.16)$$

where, $\omega_p = \sqrt{\frac{n_{eff}\cdot e^2}{m_{eff}\cdot\varepsilon_0}}$ and $\gamma = 1/\tau$. Thus, for $\omega < \omega_p$ the real part of permittivity is negative.

1.5.2 Lorentz Oscillator Model

The Lorentz oscillator model, involves modeling an electron (bound) as a driven damped harmonic oscillator. In this model the electron is connected to the nucleus via a hypothetical spring with spring constant C. The driving force is the oscillating electric field. The source of the damping force is not specified, but is present so that the oscillations don't go infinite when the driving force is at the resonant frequency. Let's say the driving oscillating electric field is $\mathbf{E} = \mathbf{E_0}\, e^{-i\omega t}$. The damping force is velocity-dependent, described by damping coefficient γ (units of γ is chosen such that force = γmv)

$$\mathbf{F}_{net} = m\ddot{\mathbf{x}}$$

$$\mathbf{F}_{driving} + \mathbf{F}_{spring} + \mathbf{F}_{damping} = m\ddot{\mathbf{x}}$$

$$q\mathbf{E_0}\, e^{-i\omega t} - C\mathbf{x} - \gamma m\dot{\mathbf{x}} = m\ddot{\mathbf{x}}$$

$$\ddot{\mathbf{x}} + \gamma\dot{\mathbf{x}} + \frac{C}{m}\mathbf{x} = \frac{q}{m}\mathbf{E_0}\, e^{-i\omega t}$$

Let, $\omega_0^2 = C/m$,

$$\ddot{\mathbf{x}} + \gamma\dot{\mathbf{x}} + \omega_0^2\mathbf{x} = \frac{q}{m}\mathbf{E_0}\, e^{-i\omega t}$$

Let us take solution as, $\mathbf{x}^* = \mathbf{x_0}\, e^{i\varphi} e^{-i\omega t}$

$$\mathbf{x}^* = \mathbf{x_0^*}\, e^{-i\omega t} \text{ (The phase } \varphi \text{ is lumped in with complex } x_0^* = x_0\, e^{i\varphi})$$

Thus, $$\dot{\mathbf{x}}^* = -i\omega \cdot \mathbf{x_0^*}\, e^{-i\omega t}$$

and $$\ddot{\mathbf{x}}^* = (-i\omega)^2 \cdot \mathbf{x_0^*}\, e^{-i\omega t}$$

Plugging these values in the Eqn. of motion

$$(-i\omega)^2 \cdot \mathbf{x_0^*}\, e^{-i\omega t} + \gamma\left(-i\omega \cdot \mathbf{x_0^*}\, e^{-i\omega t}\right) + \omega_0^2\left(\mathbf{x_0^*}\, e^{-i\omega t}\right) = \frac{q}{m}\mathbf{E_0}\, e^{-i\omega t}$$

$$\mathbf{x_0^*}(-\omega^2 - i\omega\gamma + \omega_0^2) = \frac{q}{m}\mathbf{E_0}$$

$$\mathbf{x_0^*} = \frac{q}{m}\mathbf{E_0} \cdot \frac{1}{\omega_0^2 - \omega^2 - i\omega\gamma}$$

This is complex amplitude of electron's motion. It just means there is a time delay (phase shift) between the driving electric field and the response of the electron's motion. With the explicit time dependence added back in, we have:

$$\mathbf{x}^* = \frac{q}{m}\mathbf{E_0} \cdot \frac{1}{\omega_0^2 - \omega^2 - i\omega\gamma}\, e^{-i\omega t}$$

The complex dipole moment induced by an electron moving like this in an atom (with the nucleus at the origin, stationary so it doesn't contribute to the dipole moment) is given by:

$$\mathbf{p} = \sum q_j \mathbf{r_j}$$

$$\mathbf{p}^* = q \cdot \frac{q}{m} E_0 \cdot \frac{1}{\omega_0^2 - \omega^2 - i\omega\gamma}\, e^{-i\omega t}\, \hat{x}$$

$$p^* = \frac{q^2 E_0}{m} \cdot \frac{1}{\omega_0^2 - \omega^2 - i\omega\gamma}\, e^{-i\omega t}$$

The Polarization **P** is the dipole moment per unit volume. If we assume that there are N electrons per unit volume, each acting with the same dipole moment as given above, then the complex polarization is given by multiplying the last equation by N:

$$P^* = \frac{Nq^2 E_0}{m} \cdot \frac{1}{\omega_0^2 - \omega^2 - i\omega\gamma}\, e^{-i\omega t}$$

$$P^* = \frac{Nq^2}{m} \cdot \frac{1}{\omega_0^2 - \omega^2 - i\omega\gamma} \cdot \left(E_0\, e^{-i\omega t}\right)$$

$$P^* = \frac{Nq^2}{m} \cdot \frac{1}{\omega_0^2 - \omega^2 - i\omega\gamma} \cdot E$$

The susceptibility is defined by $\mathbf{P} = \varepsilon_0 \chi \mathbf{E}$, thus,

$$\chi^* = \frac{Nq^2}{m\varepsilon_0} \cdot \frac{1}{\omega_0^2 - \omega^2 - i\omega\gamma}$$

The quantity $\frac{Nq^2}{m\varepsilon_0}$ has the units of frequency squared, similar to square of Drude angular plasma frequency ω_p^2 . Because it happens to also be the frequency a plasma will naturally oscillate at if the positive and negative charges in the plasma are offset from each other. This oscillation is of bound charge, thereby it is defined as Lorentz angular plasma frequency,

$$\omega_{pl} = \sqrt{\frac{Nq^2}{m\varepsilon_0}}$$

Thus,

$$\chi^* = \frac{\omega_{pl}^2}{\omega_0^2 - \omega^2 - i\omega\gamma}$$

And because the susceptibility and the permittivity (dielectric constant) are related via $\varepsilon_r = 1 + \chi$, thus,

$$\varepsilon_r^* = 1 + \frac{\omega_{pl}^2}{\omega_0^2 - \omega^2 - i\omega\gamma}$$

$$\varepsilon_r' - i\varepsilon_r'' = \left(1 + \frac{\omega_{pl}^2(\omega_0^2 - \omega^2)}{(\omega_0^2 - \omega^2)^2 + \omega^2\gamma^2}\right) - i\left(\frac{\omega_{pl}^2\omega\gamma}{(\omega_0^2 - \omega^2)^2 + \omega^2\gamma^2}\right) \qquad (1.17)$$

when $\omega = \omega_0$, a resonant condition is achieved, and near narrow band of resonant frequency for $\omega > \omega_0$, the real part of permittivity become negative. This negative permittivity behaviour is mainly caused by dielectric resonance of dipoles, different from the formally discussed plasma-like negative permittivity, which was mainly caused by plasmonic oscillation of free charge carriers.

1.5.3 Drude-Lorentz model

All materials composes both free as well as bound charge carriers (electrons). Therefore, its response in time varying electric filed should be studied in combination of both Drude Model and Lorentz Oscillator model. The combination of both models is known as Drude-Lorentz Oscillator model or simply, Drude-Lorentz model. Thus, the real part of dielectric constant of materials according to Drude-Lorentz model can be written as:

$$\varepsilon_r' = 1 - \frac{\omega_p^2}{\omega^2 + \gamma^2} + \frac{\omega_{pl}^2(\omega_0^2 - \omega^2)}{(\omega_0^2 - \omega^2)^2 + \omega^2\gamma^2} \qquad (1.18)$$

Thus, the materials may show negative permittivity via two mechanisms: by plasmonic oscillation of free charge carriers or by dielectric resonance, i.e., resonance of dipoles' oscillation near resonant frequency in ferroelectric materials.

1.6 Motivation of the work

In recent years, the material having negative permittivity (ε) or/and permeability (μ) have been extensively explored. In the beginning the concept for achieving/obtaining negative permittivity (ε) or/and permeability (μ) was solely theoretical. Later it was realised in artificially designed/composed metamaterials, which consists artificially composed periodic arrays of metallic units, rarely seen in natural materials. As mentioned above, the recent studies towards the development of metamaterials and realization of negative permittivity (ε) or/and permeability (μ) in natural materials highlighted the necessity of percolating metallic/conducting pathways in ceramic- or polymer-matrix composite(s). The critical percolating structures of building blocks brings challenges for composites to achieve microscopic (at atomic/molecular) level homogeneity that is needed to be used as coatings, film, or even other lower-dimensional materials or devices. This challenge can be overcome by realizing negative permittivity in mono-phase materials which is desirable for the miniaturization of the devices [96].

Investigations done in the recent past have exhibited that negative permittivity can be tuned by charge carrier concentration solely, overrides the necessity of critical percolating structures and their building block. To establish a relationship between negative permittivity and electrons concentration it is important to realize desirable negative dielectric permittivity in single-phase materials. It is well known that the charge (electron/hole) carrier concentration of single-phase materials can be manipulated by processing conditions and doping. Finding a single-phase material showing negative permittivity is a challenging task and very few reports

were available. Further, it is reported that negative permittivity depends on external parameters such as frequency and magnitude of the field and temperature. In most of the studies, negative permittivity has been studied as a function of the frequency and magnitude of an applied electric field. Study of negative permittivity as a function of temperature has rarely been made.

From the extensive literature survey we have come to know that the single phase materials which have shown negative permittivity in kHz to MHz frequency range are transition metals based perovskite oxides (ABO_3) such as $PrMnO_3$, $LaSrMnO_3$, $LaCoEuTiO_3$, $LaFeO_3$, $GdFeO_3$,and $LaBaCoO_3$ [158–163]. Except La_2NiO_4 [164], no other system having general A_2BO_4 (Layered Perovskites or Ruddlesden-Popper) has been reported as negative permittivity material. A_2BO_4 is a two-dimensional perovskite like layer structure, in this structure it is easy to implant ions as dopants into the host lattice and hence manipulate its physical and chemical properties. The Sr_2MnO_4 is A_2BO_4 layered perovskite. The multivalency of Mn cation offers the opportunity to tune its oxidation state via optimum dopant and its concentration, which may change electrical properties further. The study of phase diagram of system $Sr - Mn - O$ has shown that Sr_2MnO_4 is a metastable compound, it is stable only between 1350 ^oC to 1680 ^oC [165]. Therefore, synthesis of pure Sr_2MnO_4 and its stabilization at low temperature (below 1350 ^oC) is challenge task. Attempts have been made to synthesized compositions of the La doped $La_xSr_{2-x}MnO_4$, but only synthesis of the compositions in the range $0.25 \leq x \leq 0.7$ could be possible [48]. Therefore, in the view of above-mentioned challenges and to explore the possibility of Sr_2MnO_4 as negative permittivity material, in this thesis work efforts have been made to synthesize doped Sr_2MnO_4 and study phase stability and negative dielectric properties using solid state ceramic route. To tailor observed negative dielectric properties, a few compositions of La (at Sr), Sn (at Mn) and Nb (at Mn) systems for the first time have been synthesized by the same procedure. The effect of

selected dopants on phase stability, structure, microstructure and negative permittivity behaviour are studied in detail. Further, it is worth mentioning here that to study explicitly role of the dopant, processing parameters (calcination and sintering temperature and time) were kept same for all the samples. Systems, compositions, sample code and imported investigations made in this work are presented below;

Table 1.2 Synthesized compositions, Sample Codes and Important investigation properties.

System	Compositions	Sample Code	Important investigation Properties
Sr_2MnO_4	---	SM4 (cooling rate 4 °C/min) SM8 (cooling rate 8 °C/min) SM12 (cooling rate 12 °C/min) SMQ (quenching)	Effect of cooling rate in phase stability and electrical properties of pure Sr_2MnO_4
$La_xSr_{2-x}MnO_4$	$La_{0.3}Sr_{1.7}MnO_4$ $La_{0.5}Sr_{1.5}MnO_4$ $La_{0.7}Sr_{1.3}MnO_4$	LSM3 LSM5 LSM7	Phase stability and Negative permittivity behavior
$Sr_2Mn_{1-x}Sn_xO_4$	$Sr_2Mn_{0.7}Sn_{0.3}O_4$ $Sr_2Mn_{0.5}Sn_{0.5}O_4$ $Sr_2Mn_{0.3}Sn_{0.7}O_4$ $Sr_2Mn_0Sn_1O_4$	SMS3 SMS5 SMS7 SMS10	Phase stability and Negative permittivity behavior
$Sr_2Mn_{1-x}Nb_xO_4$	$Sr_2Mn_{0.9}Nb_{0.1}O_4$ $Sr_2Mn_{0.8}Nb_{0.2}O_4$ $Sr_2Mn_{0.7}Nb_{0.3}O_4$ $Sr_2Mn_{0.6}Nb_{0.4}O_4$ $Sr_2Mn_{0.5}Nb_{0.5}O_4$	SMN1 SMN2 SMN3 SMN4 SMN5	Phase stability and Negative permittivity behavior